DESY 13-165
LPN 13-060

September 2013

arXiv:1309.5311v1 [hep-ph] 20 Sep 2013

Phenomenology of threshold corrections for inclusive jet production at hadron colliders

M.C. Kumar[a] and S. Moch[a,b]

[a] *II. Institut für Theoretische Physik, Universität Hamburg*
Luruper Chaussee 149, D–22761 Hamburg, Germany

[b] *Deutsches Elektronensynchrotron DESY*
Platanenallee 6, D–15738 Zeuthen, Germany

Abstract

We study one-jet inclusive hadro-production and compute the QCD threshold corrections for large transverse momentum of the jet in the soft-gluon resummation formalism at next-to-leading logarithmic accuracy. We use the resummed result to generate approximate QCD corrections at next-to-next-to leading order, compare with results in the literature and present rapidity integrated distributions of the jet's transverse momentum for Tevatron and LHC. For the threshold approximation we investigate its kinematical range of validity as well as its dependence on the jet's cone size and kinematics.

We study the hadro-production of jets focusing on one-jet inclusive cross sections. This important scattering process probes parton interactions at very high scales and has been measured at the LHC as well as at the Tevatron collider in the past with very good accuracy [1–4]. At large momentum transfer the available jet cross section data have not only allowed to set limits in the TeV range on the scales of various models for new physics, but have also offered access to the determination of a number of parameters in Quantum Chromodynamics (QCD). These include the strong coupling constant α_s as well as the gluon distribution in the proton at medium to large values of the parton momentum fractions x.

In all cases, precise theoretical predictions for the measured rates are an essential prerequisite and demand good control of the higher order QCD corrections in particular. It is well-known that these can be sizable and, moreover, are dominated by soft gluon emission in the kinematical region where the transverse momentum of the observed jet is large. At such boundary of phase space the imbalance between virtual corrections and real emission contributions gives rise to large logarithms which need to be controlled to high orders in perturbation theory and, potentially, require resummation. While the exact next-to-leading order (NLO) results to the $2 \to 2$ parton scattering process underlying the one-jet inclusive hadro-production are available since long, the computation of the next-to-next-to-leading order (NNLO) cross section predictions for $2 \to 2$ parton scattering is yet to be completed. In this situation, the threshold logarithms for the one-jet inclusive cross section have been used as a means of estimating the size of the exact NNLO QCD corrections [5] and all-order resummation of soft gluon effects at large transverse momentum of the identified jet has been achieved [6–8]. Recently, the NNLO QCD corrections in the purely gluonic channel to one-jet inclusive and di-jet production at hadron colliders has been performed [9].

In the present paper we perform a phenomenological study of threshold corrections to the inclusive jet production at both, Tevatron and LHC for the rapidity integrated transverse momentum distributions of the jets. To that end, we compute those threshold logarithms in the soft-gluon resummation formalism [10, 11] and compare our results at next-to-leading logarithmic (NLL) accuracy with the available literature [5]. Given the widespread use of those QCD corrections, e.g., in experimental analysis of one-jet inclusive data [12, 13] and in the determination of parton distribution functions (PDFs) from global fits [14–16], we are particularly interested in assessing the kinematical range of validity of the NLL threshold logarithms.

For hadro-production of jets the precise definition of the threshold is an important issue, because the boundary of phase space for soft gluon emission depends on the details of jet definition, i.e., on the jet algorithm, on the jet's cone size and on assumptions of the jet's mass. As we will see, the resummation of threshold logarithms in [5] assumes massless jets in the small cone approximation, see [8]. In order to scrutinize the threshold approximation, we perform a comparison to the exact QCD results at NLO, available e.g., through the programs `NLOJET++` [17, 18] or `MEKS` [19]. We find that threshold corrections provide a valid description of the parton dynamics, although, within a kinematical range being limited to rather large transverse momenta of jet and to very small jet cone sizes. Since the latter turn out to be typically much smaller than the currently chosen values at LHC and Tevatron, the dependence on finite cone sizes, which is unaccounted for in [5], introduces a large additional systematic uncertainty in the threshold approximation. This is unlike the case of soft-gluon resummation for single-particle inclusive hadro-production at high transverse momentum [20, 21] or for heavy-quark hadro-production (see, e.g., [22–24]), where soft-gluon emission is considered relative to a final state composed of on-shell particle(s) and the threshold logarithms are found to provide extremely precise predictions through NNLO.

We are considering the following process in proton (anti-)proton collisions at hadron colliders,

$$P + P(\bar{P}) \to J + X\,, \tag{1}$$

where J denotes the observed jet and X the system recoiling against J. At the parton level, a total of 9 different subprocesses contributes, namely,

$$\begin{aligned}
q(p_1) + q'(p_2) &\to q(p_3) + q'(p_4)\,,\\
q(p_1) + \bar{q}(p_2) &\to q'(p_3) + \bar{q}'(p_4)\,,\\
q(p_1) + \bar{q}(p_2) &\to q(p_3) + \bar{q}(p_4)\,,\\
q(p_1) + q(p_2) &\to q(p_3) + q(p_4)\,,\\
q(p_1) + \bar{q}'(p_2) &\to q(p_3) + \bar{q}'(p_4)\,,\\
q(p_1) + \bar{q}(p_2) &\to g(p_3) + g(p_4)\,,\\
q(p_1) + g(p_2) &\to q(p_3) + g(p_4)\,,\\
g(p_1) + g(p_2) &\to q(p_3) + \bar{q}(p_4)\,,\\
g(p_1) + g(p_2) &\to g(p_3) + g(p_4)\,.
\end{aligned} \tag{2}$$

The Mandelstam invariants are $s = (p_1 + p_2)^2$, $t = (p_1 - p_3)^2$ and $u = (p_2 - p_3)^2$. It is to be noted that either of the partons in the final state can give rise to the observable jet and the other will be inclusive, implying that the observable can be computed either by symmetrizing the matrix elements between t and u or, alternatively, by running the jet-algorithm while doing the phase space integration. With these Mandelstam invariants, the relation $s_4 = s + t + u \geq 0$ holds where s_4 is the invariant mass of the system recoiling against the observed jet and $s_4 = 0$ at threshold.

The perturbative expansion of the partonic cross section $\hat{\sigma}$ in powers of the strong coupling constant α_s reads

$$\hat{\sigma} = \sum_{l=0}^{\infty} \hat{\sigma}^{(l)}\,, \tag{3}$$

where $\hat{\sigma}^{(0)}$ denotes the Born term. At higher orders the parton cross section $\hat{\sigma}^{(l)}$ contains plus-distributions of the type $\alpha_s^l\,[\ln^{2l-1}(s_4/p_T^2)/s_4]_+$ that lead to the Sudakov logarithms upon integration. In a physical interpretation s_4 denotes the additional energy carried away by real emission of soft gluons above the partonic threshold.

The generic l-loop expanded resummed results can be written as

$$\frac{d^2\hat{\sigma}^{(l)}}{dt\,du} = \sum_{k=0}^{2l-1} C_{l,k} \left[\frac{\ln^{(2l-1)-k}\left(s_4/p_T^2\right)}{s_4}\right]_+ + C_{l,\delta}\delta\left(s_4\right) + O\left(s_4\right)\,, \tag{4}$$

and at each loop order, the coefficients $C_{l,0}$ determine the leading logarithm (LL), the coefficients $C_{l,1}$ determine the NLL contributions and so on. It is well-established, that the threshold logarithms exponentiate and at the differential level (one-particle inclusive kinematics [25]) this exponentiation has been performed to NLL accuracy in [5], where the resummed result has been used to generate the results in fixed-order perturbation theory through NNLO.

The resummation is based on the factorization of the partonic cross section near threshold into various functions, each of which organizes the large corrections stemming from a particular

region of phase space. The full dynamics of collinear gluon emission from initial or final state partons are summarized in so-called jet functions $\mathcal{J}^I$ and $\mathcal{J}^F$ which contain all LL and some NLL enhancements. Additional soft gluon dynamics at NLL accuracy which are not collinear to one of the external partons are summarized by the soft function S, which is governed by anomalous dimension Γ_S [6, 10]. Finally, the effects of off-shell partons are collected in a so-called hard function H, where both H and S are matrices in the space of color configurations for the respective underlying $2 \to 2$ scattering process in Eq. (2).

The resummation is conveniently carried out in the space of moments N. The formal definition of Laplace moments as

$$\tilde{f}(N) = \int \frac{ds_4}{s} e^{-Ns_4/s} f(s_4/s)\,, \tag{5}$$

establishes the correspondence between the plus-distributions for $s_4 \to 0$ and the moments $N \to \infty$, that is $[\ln^{2l-1}(s_4/p_T^2)/s_4]_+ \leftrightarrow \ln^{2l} N$, see, e.g., [26] for details. Thus, the parton level resummed cross section for a generic subprocess in Eq. (2) is given by [5, 25]

$$\begin{aligned}
d\hat{\sigma}^{\rm res}_{12\to 34}(N) \;=\;& \exp\left[-\sum_{a=1,2} 2\int_{\mu_F}^{2p_a\cdot\zeta} \frac{d\mu}{\mu} C_{(f_a)} \frac{\alpha_s(\mu^2)}{\pi} \ln N_a\right] \\
&\times \exp\left[\sum_{a=1,2} \mathcal{J}^I_a(N_a)\right] \times \exp\left[\sum_{b=3,4} \mathcal{J}^F_b(N)\right] \\
&\times \exp\left[2\sum_{a=1,2}\int_{\mu_F}^{p_T} \frac{d\mu}{\mu}\gamma_a[\alpha_s(\mu^2)]\right] \times \exp\left[4\int_{\mu_R}^{p_T} \frac{d\mu}{\mu}\,\beta(\alpha_s(\mu^2))\right] \\
&\times {\rm Tr}\Bigg\{ H(\alpha_s(\mu_R^2))\,\bar{P}\exp\left[\int_{p_T}^{p_T/N} \frac{d\mu}{\mu}\,\Gamma_S^\dagger(\alpha_s(\mu^2))\right] \\
&\times S(\alpha_s(p_T^2/N^2))\,P\exp\left[\int_{p_T}^{p_T/N} \frac{d\mu}{\mu}\,\Gamma_S(\alpha_s(\mu^2))\right]\Bigg\}\,,
\end{aligned} \tag{6}$$

where the trace operation acts on the matrices S, H and Γ_S in color space and P, $\bar{P}$ denote (complex) ordered matrix products. The function β is the standard QCD beta function, $\gamma_q = (\alpha_s/\pi)(3C_F/4)$ and $\gamma_g = (\alpha_s/\pi)(\beta_0/4)$ are the anomalous dimensions for quarks and gluons needed to 1-loop accuracy here. $C_{(f_a)}$ is the quadratic Casimir operator with $C_f = C_F = (N_c^2-1)/(2N_c)$ for an external quark/antiquark and $C_f = C_A = N_c$ for an external gluon with N_c being the number of colors. The renormalization and factorization scale are given by μ_R and μ_F. Moreover, ζ_μ is a dimensionless vector specifying the kinematics, see [25], so that in single-particle inclusive kinematics it can be taken as $\zeta_\mu = p_J/p_T$ and, likewise, the moments N_a $(a = 1,2)$ are given by $N_1 = N(-u/s)$ and $N_2 = N(-t/s)$.

The initial state functions $\mathcal{J}^I_a$ generate the LL and some NLL logarithms as a double integral over the cusp anomalous dimension $A^{(f_a)}(\alpha_s) = C_f\left((\alpha_s/\pi) + (K/2)(\alpha_s/\pi)^2\right)$ with $K = C_A(67/18 - \pi^2/6) - 5n_f/9$ and n_f being the number of quark flavors. In Mellin space, the $\mathcal{J}^I_a$

are given by

$$\mathcal{J}_a^I(N_a) = -\int_0^1 dz \frac{z^{N_a-1}}{1-z}\left[\int_{(1-z)^2}^1 \frac{d\lambda}{\lambda} A^{(f_a)}[\alpha_s(\lambda(2p_a.\zeta)^2)] + \frac{1}{2}\nu^{(f_a)}[\alpha_s((1-z)^2(2p_a.\zeta)^2)]\right], \quad (7)$$

where $\nu^{(f_a)} = 2C_{(f_a)}(\alpha_s/\pi)$.

The final state jet functions $\mathcal{J}_b^F$ describe both, soft and hard, radiation collinear to the outgoing partons giving rise to the observed jet and the inclusive remainder recoiling against the observed jet. The $\mathcal{J}_b^F$ are given by

$$\begin{aligned}\mathcal{J}_b^F(N) &= \int_0^1 dz \frac{z^{N-1}}{1-z}\left[\int_{(1-z)^2}^{(1-z)} \frac{d\lambda}{\lambda} A^{(f_b)}[\alpha_s(\lambda p_T^2)]\right. \\ &\qquad \left. + B_b^{(1)}[\alpha_s((1-z)p_T^2)] + B_b^{(2)}[\alpha_s((1-z)^2 p_T^2)]\right], \end{aligned} \quad (8)$$

where $B_{(q)}^{(1)} = (-3C_F/4)(\alpha_s/\pi)$, $B_{(q)}^{(2)} = C_F[\ln(2\nu_q)-1](\alpha_s/\pi)$, $B_{(g)}^{(1)} = (-\beta_0/4)(\alpha_s/\pi)$ and $B_{(g)}^{(2)} = C_A[\ln(2\nu_g)-1](\alpha_s/\pi)$, with β_0 being the first coefficient of the QCD beta function. Here, the $\nu_i = (\beta_i.n)^2/|n|^2$ are gauge dependent terms, where $\beta_i = p_i\sqrt{2/s}$ are the particle velocities and n is the axial gauge vector chosen such that $p_i \cdot \zeta = p_i \cdot n$. As we have discussed already above, it is in the expression for $\mathcal{J}_b^F$, that any dependence on the jet definition, in particular on the jet's cone size R is lacking. This has important consequences, as any finite R dependence will alter the resummed cross section at LL accuracy, since the large logarithms generated by the collinear contributions in $\mathcal{J}_b^F$ are actually regularized by the cone size and instead give rise to logarithmic terms in R in the perturbative cross section, see also [8]. Thus, Eq. (6) holds in the limit $R \to 0$ and the numerical impact of such approximation will be illustrated in what follows when comparing to NLO results for R values typically used in jet analysis.

To investigate this further requires considering the differences between the threshold corrections and the fixed order results by going into the details of their computation, in particular the jet algorithm being used in the NLO computation. The higher order QCD corrections crucially depend on the value of the parameter R (cone size) used in the jet algorithm. A parton in the final state resulting from a hard scattering is completely different from a jet that is observed in the experiments. At LO the transverse momenta of the two partons in the final state, which eventually hadronize and form two jets, balance each other and are well separated in the rapidity-azimuthal angular plane. Hence the LO theory predictions are insensitive to the value of R. However, at NLO and beyond there are additional partons in the final state. Whenever two or more partons fall within a cone of size R, their momenta are combined in a scheme to form a new object which eventually hadronizes to form a single jet. The larger the value of R, the larger will be the number of jet events thus counted. Thus, the higher order QCD corrections for inclusive jet production depend on the value of R and, in fact, increase with R. The computation of the threshold corrections on the other hand is based on the phase space slicing underlying Eq. (6) and involves the s_4 integration which captures the information of the additional gluon radiation at higher orders. However, there is no explicit additional gluon radiation in the final state that can be subjected to a jet algorithm and can eventually be associated with a parton inside a cone of size R to form a single jet. Thus the threshold corrections Eq. (6) carry no dependence on R.

Finally, the soft and the hard functions carry the information about the color exchange in the specific parton scattering process and account for the associated soft gluon effects in QCD hard scattering. In our analytical computation we use Symbolic Manipulation program FORM [27] and the related color package [28] for color algebra. Following [29] we choose for a $qq \to qq$ process $ij \to kl$ the t-channel color basis

$$c_1 = \delta_{ik}\,\delta_{jl}\,, \qquad c_2 = t^c_{ki}\,t^c_{jl}\,, \tag{9}$$

where t^c_{ij} are the generators of $SU(3)$ group in the fundamental representation and $N_c = 3$ is the number of colors, so that the tree level soft function for this basis given by $S^{(0)}_{qq\to qq} = \mathrm{diag}(9,2)$. Likewise, the t-channel color bases for the $qg \to qg$ process $ij \to kl$ are given by

$$c_1 = \delta_{ik}\delta_{jl}\,, \qquad c_2 = d^{jlc}t^c_{ki}\,, \qquad \text{and} \qquad c_3 = i\,f^{jlc}\,t^c_{ki}\,, \tag{10}$$

with the tree level soft function $S^{(0)}_{qg\to qg} = \mathrm{diag}(24, 20/3, 12)$ and for a $gg \to gg$ process $ij \to kl$ by

$$\begin{aligned}
c_{1,2} &= \frac{i}{4}[f^{ijm}d^{klm} \mp d^{ijm}f^{klm}]\,,\\
c_3 &= \frac{i}{4}[f^{ikm}d^{jlm} + d^{ikm}f^{jlm}]\,,\\
c_4 &= \frac{1}{8}\delta_{ik}\delta_{jl}\,,\\
c_5 &= \frac{3}{5}d^{ikn}\,d^{jln}\,,\\
c_6 &= \frac{1}{3}f^{ikn}\,f^{jln}\,,\\
c_7 &= \frac{1}{2}\left(\delta_{ij}\delta_{kl} - \delta_{il}\delta_{jk}\right) - \frac{1}{3}f^{ikn}\,f^{jln}\,,\\
c_8 &= \frac{1}{2}\left(\delta_{ij}\delta_{kl} + \delta_{il}\delta_{jk}\right) - \frac{1}{8}\delta_{ik}\delta_{jl} - \frac{3}{5}d^{ikn}\,d^{jln}\,.
\end{aligned} \tag{11}$$

In the latter case, the soft function assumes the form $S^{(0)}_{gg\to gg} = \mathrm{diag}(5,5,5,1,8,8,20,27)$ for this basis. All other $2 \to 2$ processes in Eq. (2) are obtained by crossing and together with the corresponding hard functions $H^{(0)}_{ij\to kl}$ the trace $\mathrm{Tr}(H^{(0)}S^{(0)})$ is proportional to the Born cross section.

The resummation of the soft color exchange requires the computation of the soft anomalous dimensions [10], where the 1-loop expression $\Gamma^{(1)}_S$ suffices to NLL accuracy. The soft anomalous dimension is gauge dependent and to 1-loop level it can be expressed in color space as

$$\Gamma_{S,\,IJ} = \Gamma^{(1)}_{S,\,IJ} + \delta_{IJ}\,\frac{\alpha_s}{\pi}\sum_{i=1}^{4} C_{(f_i)}\frac{1}{2}\left[-\ln(2\nu_i) + 1 - i\pi\right]\,, \tag{12}$$

where the gauge dependent terms ν_i are as defined previously. For the process $qq \to qq$ and in the basis Eq. (9) it is given by

$$\Gamma^{(1)}_{S,qq\to qq} = \frac{\alpha_s}{\pi}\begin{bmatrix} -\frac{1}{3}(T+U) + \frac{8}{3}U & 2U \\ \frac{4}{9}U & \frac{8}{3}\,T \end{bmatrix}\,, \tag{13}$$

where $T = \ln\left(\frac{-t}{s}\right) + i\pi$ and $U = \ln\left(\frac{-u}{s}\right) + i\pi$. Likewise, for the $qg \to qg$ process in the basis Eq. (10) we have

$$\Gamma^{(1)}_{S,qg\to qg} = \frac{\alpha_s}{\pi}\begin{bmatrix} \frac{13}{3}T & 0 & U \\ 0 & \frac{4}{3}T+\frac{3}{2}U & \frac{3}{2}U \\ 2U & \frac{5}{6}U & \frac{4}{3}T+\frac{3}{2}U \end{bmatrix}, \tag{14}$$

and for the subprocess $gg \to gg$, cf. Eq. (11), the block-diagonal form $\Gamma^{(1)}_{S,gg\to gg} = \mathrm{diag}(G_{3\times 3}, G_{5\times 5})$ where $G_{3\times 3} = (\alpha_s/\pi)\mathrm{diag}(3T, 3U, 3(T+U))$ and

$$G_{5\times 5} = \frac{\alpha_s}{\pi}\begin{bmatrix} 6T & 0 & -6U & 0 & 0 \\ 0 & 3T+\frac{3}{2}U & -\frac{3}{2}U & -3U & 0 \\ -\frac{3}{4}U & -\frac{3}{2}U & 3T+\frac{3}{2}U & 0 & -\frac{9}{4}U \\ 0 & -\frac{6}{5}U & 0 & 3U & -\frac{9}{5}U \\ 0 & 0 & -\frac{2}{3}U & -\frac{4}{3}U & -2T+4U \end{bmatrix}. \tag{15}$$

Within this set-up we have computed the resummed cross section in Eq. (6) for all parton channels and expand the resummed results to 2-loop level at NLL accuracy. At the 1-loop level, this determines the coefficients $C_{1,0}$ and $C_{1,1}$ in Eq. (4), while the coefficient $C_{1,\delta}$ of the $\delta(s_4)$ includes the 1-loop corrections to the hard and the soft function, $H^{(1)}$ and $S^{(1)}$ that can be extracted from the finite parts of the fixed order NLO computation. This matching is required for next-to-next-to-leading logarithmic (NNLL) contributions and the necessary formulae in various kinematics have been derived in [20,30]. At the 2-loop level Eq. (6) determines $C_{2,0}$ and $C_{2,1}$. Starting from NNLL accuracy the coefficient $C_{2,2}$ involves the hard matching functions mentioned above, i.e., the term $C_{1,\delta}$. In the present analysis, though, we have not included these matching functions and leave them for future study.

We find that our analytical results for all parton level cross sections are in good agreement with those given in [5] except for a small difference of an overall color factor of $[N_c^2/(N_c^2-1)^2]$ at NLL level for the subprocess $gg \to q\bar{q}$. The 1-loop corrections to NLL accuracy for this subprocess are

$$\begin{aligned} s^2\frac{d^2\hat{\sigma}^{(1)}_{gg\to q\bar{q}}}{dt\,du} &= \alpha_s\hat{\sigma}^{(0)}_{gg\to q\bar{q}}\Bigg\{(4C_A-2C_F)\left[\frac{\ln\left(s_4/p_T^2\right)}{s_4}\right]_+ \\ &\quad + \left[-2C_A\ln\left(\frac{\mu_F^2}{p_T^2}\right) - (2C_F-C_A)\ln\left(\frac{p_T^2}{s}\right) - \frac{3}{2}C_F\right]\left[\frac{1}{s_4}\right]_+\Bigg\} \\ &\quad + \alpha_s^3\frac{N_c^2}{(N_c^2-1)^2}\Bigg\{-\frac{(N_c^2-1)}{2N_c^2}\frac{(t^2+u^2)}{tu}\ln\left(\frac{p_T^2}{s}\right) \\ &\quad -\frac{(N_c^2-1)}{2}\left[\frac{u^2-t^2}{tu}+\frac{2(u-t)}{s}\right]\ln\left(\frac{u}{t}\right)\Bigg\}\left[\frac{1}{s_4}\right]_+, \end{aligned} \tag{16}$$

where $\hat{\sigma}^{(0)}_{gg\to q\bar{q}}$ contains the spin and color averaged leading order (LO) matrix elements and is given by

$$\hat{\sigma}^{(0)}_{gg\to q\bar{q}} = \alpha_s^2\left[\frac{1}{6}\,\frac{t^2+u^2}{tu} - \frac{3}{8}\frac{t^2+u^2}{s^2}\right]. \tag{17}$$

The corresponding 2-loop corrections at NLL accuracy are given by

$$
\begin{aligned}
s^2 \frac{d^2\hat{\sigma}^{(2)}_{gg\to q\bar{q}}}{dt\,du} &= \left(\frac{\alpha_s^2}{\pi}\right)\hat{\sigma}^{(0)}_{gg\to q\bar{q}}\Bigg\{\frac{1}{2}(4C_A-2C_F)^2\left[\frac{\ln^3\left(s_4/p_T^2\right)}{s_4}\right]_+ \\
&+\Bigg[3(2C_A-C_F)\left[-2C_A\ln\left(\frac{\mu_F^2}{p_T^2}\right)-(2C_F-C_A)\ln\left(\frac{p_T^2}{s}\right)-\frac{3}{2}C_F\right] \\
&+\beta_0\left(-C_A+\frac{3}{4}C_F\right)\Bigg]\left[\frac{\ln^2(s_4/p_T^2)}{s_4}\right]_+\Bigg\} \\
&+\frac{\alpha_s^4}{\pi}\frac{N_c^2}{(N_c^2-1)^2}3(2C_A-C_F)\Bigg\{-\frac{(N_c^2-1)}{2N_c^2}\frac{(t^2+u^2)}{tu}\ln\left(\frac{p_T^2}{s}\right) \\
&-\frac{(N_c^2-1)}{2}\left[\frac{u^2-t^2}{tu}+\frac{2(u-t)}{s}\right]\ln\left(\frac{u}{t}\right)\Bigg\}\left[\frac{\ln^2(s_4/p_T^2)}{s_4}\right]_+ . \qquad (18)
\end{aligned}
$$

A complete treatment of the kinematics and phase space integration can be found in [31] and the plus-distributions are defined as in [25]. We note that the relative contribution of the above subprocess $gg \to q\bar{q}$ to the total cross section is numerically very small for both Tevatron and LHC energies, hence the differences observed in Eq. (18) are numerically small in any application for collider phenomenology.

Let us now present the transverse momentum distributions of the inclusive jet at both Tevatron ($\sqrt{S} = 1.96$ TeV) and LHC ($\sqrt{S} = 7$ TeV). Since we are interested in the perturbative convergence of the coefficient functions, we convolute these functions with just a set of PDFs extracted to a certain order. In our analysis, we use CTEQ6.6 ($\alpha_s(M_Z^2) = 0.118$) [32] and ABM11 NNLO ($\alpha_s(M_Z^2) = 0.1134$) [14] PDFs. The strong coupling α_s is provided by the respective PDF sets through `LHAPDF` interface [33]. Throughout our analysis, we use the scale choice $\mu_F = \mu_R = p_T$, where p_T is the transverse momentum of the observed jet. We present our distributions for jet transverse momentum in the central rapidity region $0 \leq |y| \leq 0.5$ for LHC and $0 \leq y \leq 0.4$ for Tevatron, where the parton fluxes are dominated by parton momentum fractions x_1 and x_2 of similar order, y being the jet rapidity. Further, in the rest of the paper we use the following K-factors defined as:

$$
K^{(1)} = 1 + \frac{\sigma^{(1)}}{\sigma^{(0)}}, \qquad K^{(2)} = 1 + \frac{\sigma^{(2)}}{\sigma^{(0)}}, \qquad (19)
$$

$$
K^{(NLO)} = 1 + \frac{\sigma^{(NLO)}}{\sigma^{(0)}}, \qquad K^{(NNLO*)} = 1 + \frac{\sigma^{(NLO)} + \sigma^{(2)}}{\sigma^{(0)}}, \qquad (20)
$$

where $\sigma^{(0)}$ is the LO cross section, $\sigma^{(1)}$ and $\sigma^{(2)}$ are respectively the 1-loop and 2-loop threshold corrections expanded to only NLL accuracy and $\sigma^{(NLO)}$ is the exact NLO correction to the cross section.

As a first check, we compare our numerical results with those obtained from `FastNLO` [34,35]. In the left panel of Fig. 1, we show the comparison of LO cross sections and 1-loop threshold corrections $\sigma^{(1)}$ for Tevatron at $\sqrt{S} = 1.96$ TeV center-of-mass (cms) energy and in the right panel of Fig. 1 the corresponding K-factor $K^{(1)}$ as defined in Eq. (19). Similar plots for 2-loop threshold

corrections $\sigma^{(2)}$ and the K-factors $K^{(2)}$ are presented in Fig. 2 for the Tevatron at $\sqrt{S} = 1.96$ TeV and in Fig. 3 for $\sqrt{S} = 7$ TeV LHC. In all cases, we find that our results are well in agreement with those obtained from `FastNLO`. For the 2-loop threshold corrections $\sigma^{(2)}$ this constitutes an independent check of [5] and confirms that possible differences in the analytical expressions, cf. Eq. (18), have small numerical impact.

Next, we validate the threshold corrections by comparing them with the fixed order NLO results in the perturbation theory. In Fig. 4, we present the K-factors $K^{(1)}$, $K^{(2)}$ and $K^{(NLO)}$. The NLO results for $K^{(NLO)}$ are read from the grids of `FastNLO`. In the case of LHC at $\sqrt{S} = 7$ TeV cms (left panel in Fig. 4) these are used in the CMS inclusive jet data analysis [2] together with the anti-k_t jet algorithm [36] with $R = 0.5$.

We observe in Fig. 4 that $K^{(1)}$ and $K^{(2)}$ are sizable, of the order $O(1.1)$ to $O(1.2)$ at large p_T. The high p_T region of the jet corresponds to the threshold region $s_4 = 0$, where the phase space for the gluon radiation is limited. In this region, in particular the 1-loop threshold corrections are expected to reproduce the exact fixed order NLO QCD corrections, i.e., $K^{(1)} \simeq K^{(NLO)}$, as a result of the dominance of the Sudakov logarithms in the perturbation expansion. However, as can be seen from Fig. 4, this is not quite the case. Far away, from the threshold region, at small p_T, the threshold corrections in $K^{(1)}$ are found to be larger than $K^{(NLO)}$ for $p_T < 400$ GeV and for lower p_T values (for about $p_T < 200$ GeV), even $K^{(2)}$ is found to exceed $K^{(NLO)}$. This indicates, that the 2-loop threshold corrections, as such, in this region of phase space are subject to very large theory uncertainties and cannot be used in the relevant experimental data analysis.

In order to clarify the deviations between $K^{(1)}$ and $K^{(NLO)}$ illustrated in Fig. 4 we study the dependence on R. We compute the NLO cross sections as a function of R for inclusive jet production at LHC and Tevatron. For this computation, we use `NLOJET++` program, anti-k_t jet algorithm [36] from `FastJet` [37]. and CTEQ6.6 PDFs [32]. In Figs. 5 and 6 we present our results in terms of $K^{(NLO)}$ for $\sqrt{S} = 7$ TeV and 8 TeV LHC by varying R from 0.2 to 0.7 and by considering p_T of jet as high as 2500 GeV. Likewise, Fig. 7 displays the results for the Tevatron Run II case using the anti-k_t jet algorithm and varying R from 0.2 to 0.7. As can be seen from those figures, the NLO QCD cross sections increase with the cone size R. Further, $K^{(NLO)}$ is less than unity for smaller p_T values and for smaller R values, because the $O(\alpha_s)$ QCD corrections are negative in this region. On the contrary for higher $R(> 0.4)$ values, $K^{(NLO)}$ is always greater than unity. Moreover, the NLO QCD corrections do increase by about 30% as R varies from 0.2 to 0.7, regardless of the value of p_T in the range considered here.

It is therefore quite revealing to compare these NLO corrections with the 1-loop threshold corrections as done in Figs. 5-7. There, in Fig. 5 for $\sqrt{S} = 7$ TeV LHC, $K^{(1)}$ decreases with increasing p_T up to about 800 GeV and then increases with p_T. At very large p_T the threshold logarithms are dominant and we observe for the K-factors $K^{(1)}$ and $K^{(NLO)}$ the same rising behavior in this region. Interestingly, in the high p_T region the approximation which is independent of R coincides with the exact NLO result only when the latter is computed for smaller R values of about 0.3, i.e., $K^{(1)} \simeq K^{(NLO)}$ for $R = 0.3$ for the LHC, cf. Figs. 5 and 6. Likewise, for the Tevatron the 1-loop threshold corrections are comparable to the exact NLO ones for the cone size of about $R = 0.4$ in the high p_T region, cf. Fig. 7. In Figs. 8 and 9, we present the K-factors $K^{(1)}$, $K^{(2)}$, $K^{(NLO)}$ and $K^{(NNLO*)}$ for $\sqrt{S} = 7$ TeV and 8 TeV LHC respectively for a cone size of $R = 0.7$. In summary, the absence of any dependence on the jet's cone size R in the threshold corrections implies a very large theoretical uncertainty inherent in [5].

In discussing our findings, it is worth noting here that the corresponding 2-loop threshold cor-

rections for the Tevatron illustrated in Figs. 2 and 7 have been used in the determination of the strong coupling constant from the Tevatron inclusive jet cross section data [12] by considering the jet transverse momentum in the range $50 < p_T < 145$ GeV. The corresponding theory predictions are obtained from MSTW 2008 PDF sets. In this analysis, the strong coupling constant obtained from pure NLO perturbative QCD corrections is determined to be $\alpha_s(M_Z^2) = 0.1201$ while the inclusion of the 2-loop threshold corrections has decreased its central value to $\alpha_s(M_Z^2) = 0.1161$.

Moreover, another remark to be made in the discussion of Figs. 5 and 6 is that the 1-loop threshold corrections in the low p_T region of the jet ($p_T < 500$ GeV), are much higher than the exact NLO QCD corrections computed for all values of $R < 0.7$. For improved approximations beyond NLL, it is required to systematically include also the hard matching functions $H^{(1)}$ that can be extracted from the finite parts of the virtual corrections in the NLO computation. Such an analysis, but using different kinematics, has been done in [7] wherein the logarithms of the kind $\alpha_s^k \ln^{2k}(1-x_T^2)$ are resummed at NLL accuracy. An extension to this work has also been done in [8] where the integration is done over jet mass defined in terms of the cone size R. However, for the present case using s_4 kinematics where the logarithms of type $[\ln^l(s_4/p_T^2)/s_4]_+$ are considered, the hard matching functions are expected to be small in the threshold region as they are independent of threshold logarithms and the relevant parton fluxes in this region fall rapidly.

Further necessary improvements thus concern the extension of the threshold corrections to NNLL accuracy, a proper treatment of the jet's kinematics and cone size and, of course, the completion of the exact NNLO QCD corrections [9]. Unrelated, though also necessary is inclusion of the electro-weak corrections at NLO to hadro-production of jets possibly the effect of electro-weak Sudakov logarithms, see, e.g., [38, 39].

To summarize, we have computed the threshold corrections to inclusive jet production at hadron colliders in the soft-gluon resummation formalism. We find that that our results are in agreement with those in the literature apart from few typographical errors. Furthermore, we have investigated the phenomenology of these threshold corrections by comparing them expanded to 1-loop level at NLL accuracy with the exact NLO results. We have also studied the dependence of the exact NLO results on the cone size R. These QCD threshold corrections are better comparable in the high p_T region with the exact NLO QCD corrections only when the latter are computed for smaller cone sizes, about $R = 0.3$ and $R = 0.4$ for LHC and Tevatron. For the LHC at $\sqrt{S} = 7$ TeV cms energy, our analysis indicates that applying these threshold corrections for $p_T < 500$ GeV can lead to large uncertainties and in particular potential theoretical uncertainties for $p_T < 200$ GeV. On the contrary, for higher p_T values near threshold region, they underestimate the fixed order results in the perturbation theory for typical values of R used in jet analysis at LHC experiments.

Acknowledgments

We are thankful to D. Britzger, K. Rabbertz and M. Wobisch for useful discussions on `FastNLO` and for providing us with a `FastNLO` table for 1-loop threshold corrections at Tevatron. We also thank N. Kidonakis for his comments on the analytical part of this computation.

This work has been supported by Deutsche Forschungsgemeinschaft in Sonderforschungsbereich SFB 676 and by the European Commission through contract PITN-GA-2010-264564 (*LHCPhenoNet*).

References

[1] ATLAS Collaboration, G. Aad *et al.*, Phys.Rev. **D86**, 014022 (2012), arXiv:1112.6297.

[2] CMS Collaboration, S. Chatrchyan *et al.*, Phys.Rev.Lett. **107**, 132001 (2011), arXiv:1106.0208.

[3] CDF Collaboration, T. Aaltonen *et al.*, Phys.Rev. **D78**, 052006 (2008), arXiv:0807.2204.

[4] D0 Collaboration, V. Abazov *et al.*, Phys.Rev.Lett. **101**, 062001 (2008), arXiv:0802.2400.

[5] N. Kidonakis and J. Owens, Phys.Rev. **D63**, 054019 (2001), arXiv:hep-ph/0007268.

[6] N. Kidonakis, G. Oderda, and G. F. Sterman, Nucl.Phys. **B525**, 299 (1998), arXiv:hep-ph/9801268.

[7] D. de Florian and W. Vogelsang, Phys.Rev. **D71**, 114004 (2005), arXiv:hep-ph/0501258.

[8] D. de Florian and W. Vogelsang, Phys.Rev. **D76**, 074031 (2007), arXiv:0704.1677.

[9] A. G.-D. Ridder, T. Gehrmann, E. Glover, and J. Pires, (2013), arXiv:1301.7310.

[10] H. Contopanagos, E. Laenen, and G. Sterman, Nucl. Phys. **B484**, 303 (1997), hep-ph/9604313.

[11] S. Catani, M. L. Mangano, P. Nason, and L. Trentadue, Nucl. Phys. **B478**, 273 (1996), hep-ph/9604351.

[12] D0 Collaboration, V. Abazov *et al.*, Phys.Rev. **D80**, 111107 (2009), arXiv:0911.2710.

[13] D0 Collaboration, V. M. Abazov *et al.*, Phys.Lett. **B718**, 56 (2012), arXiv:1207.4957.

[14] S. Alekhin, J. Blümlein, and S. Moch, Phys.Rev. **D86**, 054009 (2012), arXiv:1202.2281.

[15] S. Alekhin, J. Blümlein, and S. Moch, (2012), arXiv:1211.2642.

[16] A. Martin, W. Stirling, R. Thorne, and G. Watt, Eur.Phys.J. **C63**, 189 (2009), arXiv:0901.0002.

[17] Z. Nagy, Phys. Rev. **D68**, 094002 (2003), hep-ph/0307268.

[18] Z. Nagy, Phys. Rev. Lett. **88**, 122003 (2002), hep-ph/0110315.

[19] J. Gao *et al.*, Comput.Phys.Commun. **184**, 1626 (2013), arXiv:1207.0513.

[20] S. Catani, M. Grazzini, and A. Torre, Nucl.Phys. **B874**, 720 (2013), arXiv:1305.3870.

[21] D. de Florian, M. Pfeuffer, A. Schafer, and W. Vogelsang, (2013), arXiv:1305.6468.

[22] R. Bonciani, S. Catani, M. L. Mangano, and P. Nason, Nucl. Phys. **B529**, 424 (1998), hep-ph/9801375.

[23] S. Moch and P. Uwer, Phys. Rev. **D78**, 034003 (2008), arXiv:0804.1476.

[24] S. Moch, P. Uwer, and A. Vogt, Phys.Lett. **B714**, 48 (2012), arXiv:1203.6282.

[25] E. Laenen, G. Oderda, and G. F. Sterman, Phys.Lett. **B438**, 173 (1998), arXiv:hep-ph/9806467.

[26] E. Laenen and S. Moch, Phys.Rev. **D59**, 034027 (1999), arXiv:hep-ph/9809550.

[27] J. Vermaseren, (2000), arXiv:math-ph/0010025.

[28] T. van Ritbergen, A. Schellekens, and J. Vermaseren, Int.J.Mod.Phys. **A14**, 41 (1999), arXiv:hep-ph/9802376.

[29] N. Kidonakis, G. Oderda, and G. F. Sterman, Nucl.Phys. **B531**, 365 (1998), arXiv:hep-ph/9803241.

[30] R. Kelley and M. D. Schwartz, Phys.Rev. **D83**, 045022 (2011), arXiv:1008.2759.

[31] W. Beenakker, H. Kuijf, W. van Neerven, and J. Smith, Phys.Rev. **D40**, 54 (1989).

[32] P. M. Nadolsky *et al.*, Phys.Rev. **D78**, 013004 (2008), arXiv:0802.0007.

[33] M. Whalley, D. Bourilkov, and R. Group, (2005), arXiv:hep-ph/0508110.

[34] fastNLO Collaboration, M. Wobisch, D. Britzger, T. Kluge, K. Rabbertz, and F. Stober, (2011), arXiv:1109.1310.

[35] fastNLO Collaboration, D. Britzger, K. Rabbertz, F. Stober, and M. Wobisch, p. 217 (2012), arXiv:1208.3641.

[36] M. Cacciari, G. P. Salam, and G. Soyez, JHEP **0804**, 063 (2008), arXiv:0802.1189.

[37] M. Cacciari, G. P. Salam, and G. Soyez, Eur.Phys.J. **C72**, 1896 (2012), arXiv:1111.6097.

[38] S. Dittmaier, A. Huss, and C. Speckner, (2013), arXiv:1306.6298.

[39] J. H. Kühn, S. Moch, A. Penin, and V. A. Smirnov, Nucl.Phys. **B616**, 286 (2001), arXiv:hep-ph/0106298.

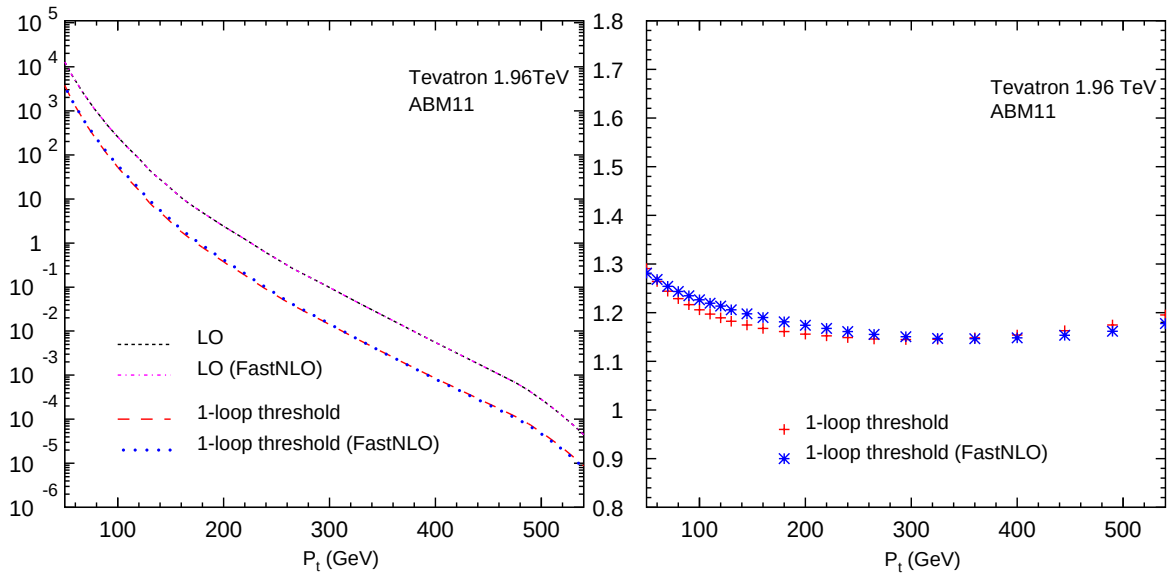

Figure 1: LO results and 1-loop threshold corrections $\sigma^{(1)}$ for the transverse momentum distribution of the jet (left) and the corresponding K-factor $K^{(1)}$ (right) at Tevatron.

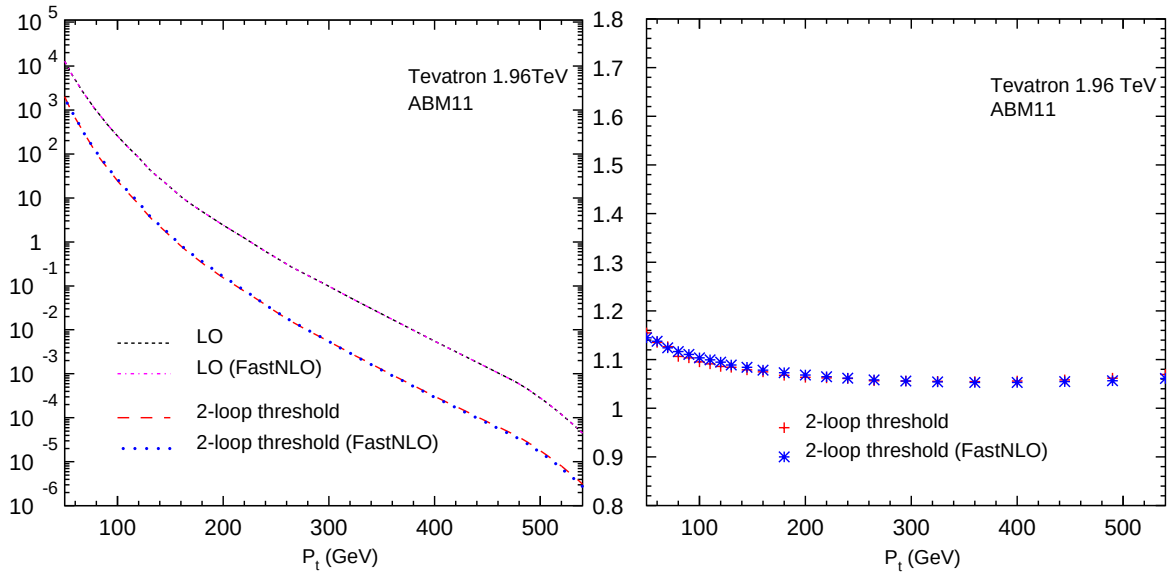

Figure 2: LO results and 2-loop threshold corrections $\sigma^{(2)}$ for the transverse momentum distribution of the jet (left) and the corresponding K-factor $K^{(2)}$ (right) at Tevatron.

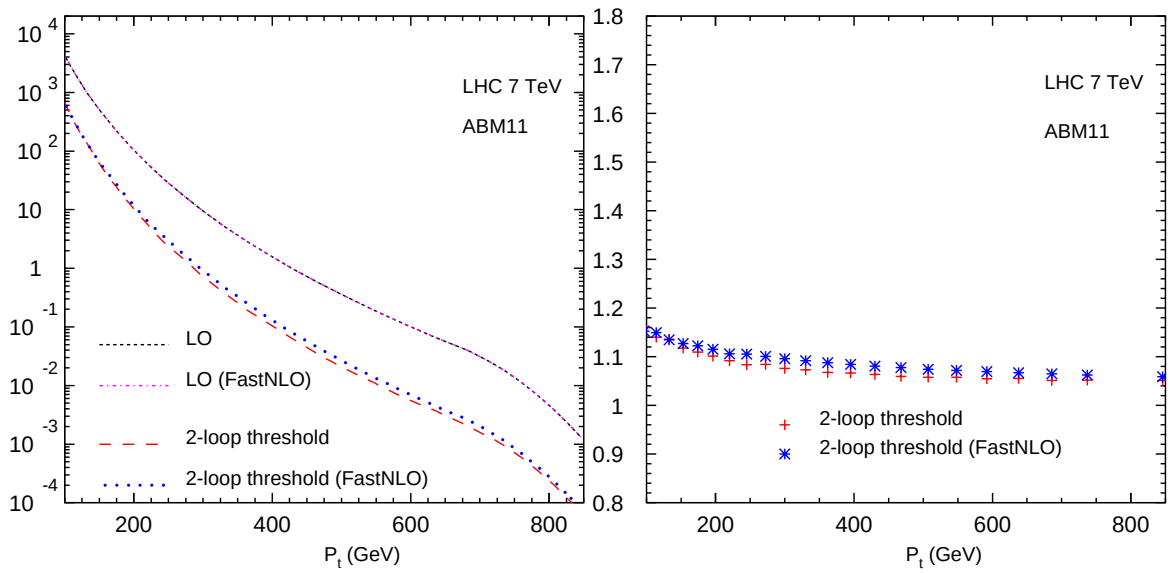

Figure 3: Same as Fig. 2 for the $\sqrt{S} = 7$ TeV LHC.

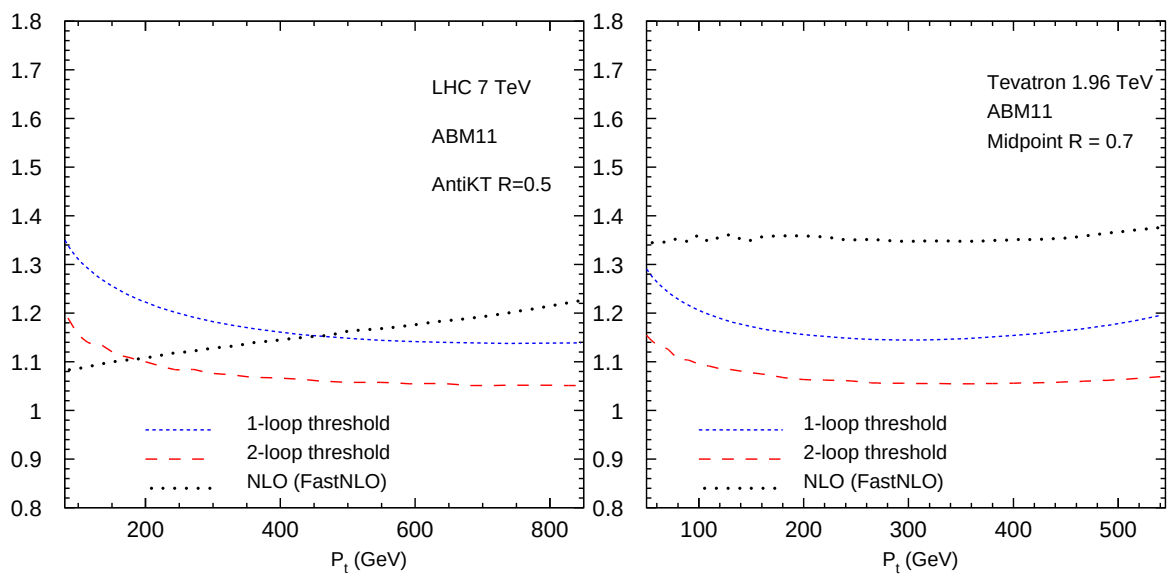

Figure 4: K-factors $K^{(1)}$, $K^{(2)}$ and $K^{(NLO)}$ defined with respect to 1-loop threshold corrections, 2-loop threshold corrections and the exact NLO results for $\sqrt{S} = 7$ TeV LHC (left) and for Tevatron (right).

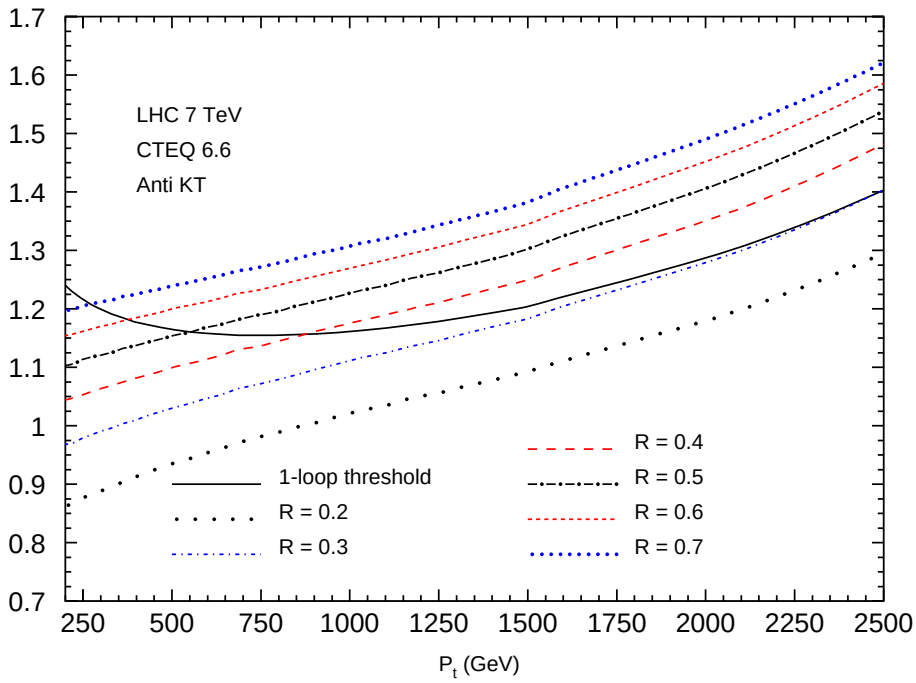

Figure 5: NLO K-factors $K^{(NLO)}$ for inclusive jet production as a function of the parameter R in the anti-k_t jet algorithm, computed for $\sqrt{S} = 7$ TeV LHC. The solid line corresponds to the one-loop threshold corrections $K^{(1)}$ at NLL accuracy.

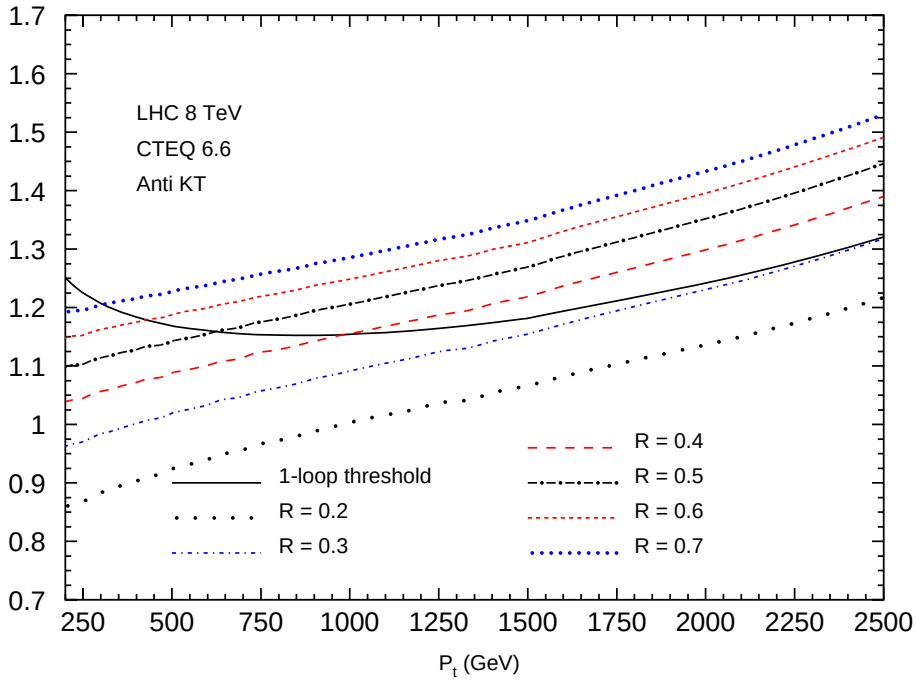

Figure 6: Same as Fig. 5 for the $\sqrt{S} = 8$ TeV LHC.

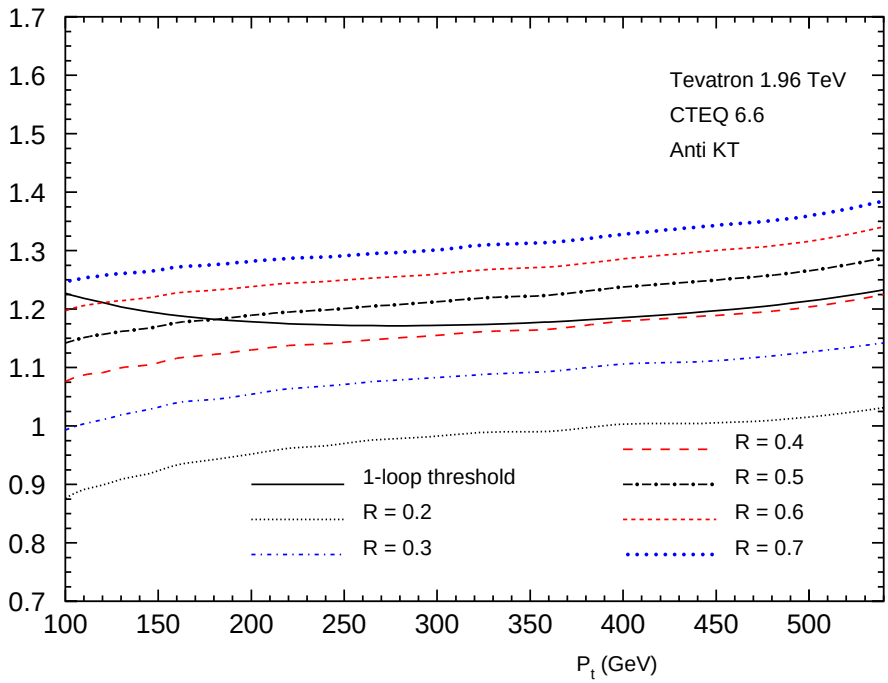

Figure 7: Same as Fig. 5 for the Tevatron.

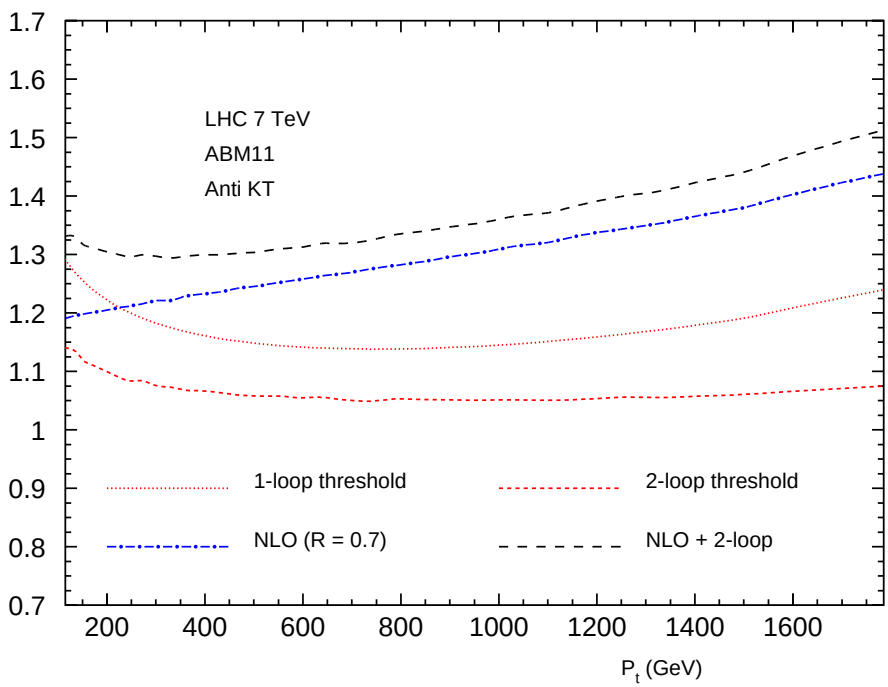

Figure 8: Comparison of K-factors $K^{(1)}$, $K^{(2)}$, $K^{(NLO)}$ and $K^{(NNLO*)}$ for 1-loop threshold, 2-loop threshold, NLO and NLO + 2-loop (NNLO*) cross sections computed for $\sqrt{S} = 7$ TeV LHC.

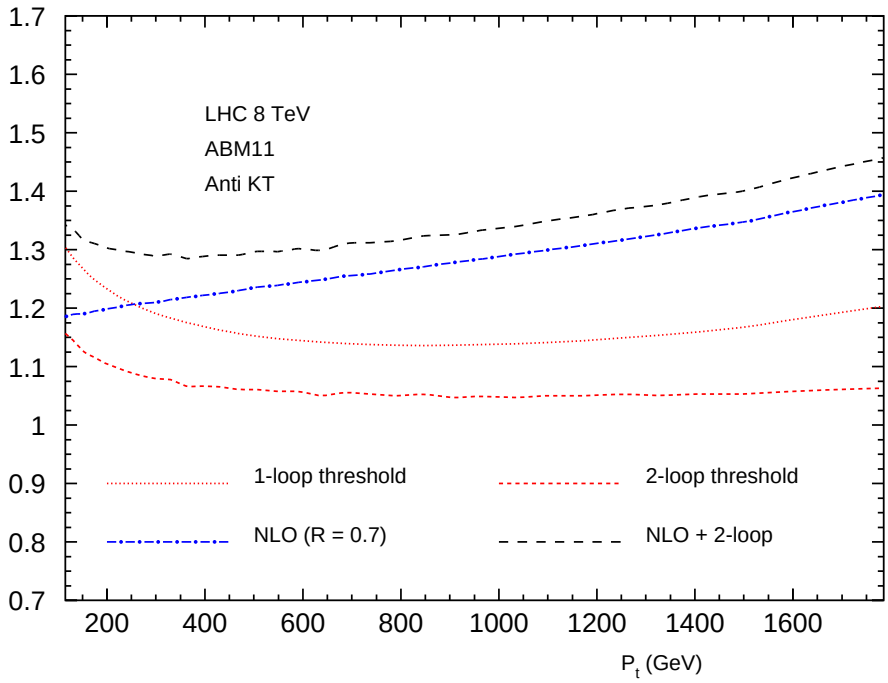

Figure 9: Same as Fig. 8 for the $\sqrt{S} = 8$ TeV LHC.